SUPPLEMENTARY INFORMATION

Composition-tuned Pt-skinned PtNi bimetallic clusters as highly efficient methanol dehydrogenation catalysts

Ting-Wei Liao[1]*ǂ, Anupam Yadav[1]ǂ, Piero Ferrari[1], Yubaio Niu[2], Xian-Kui Wei[3], Jerome Vernieres[2], Kuo-Juei Hu[1], Marc Heggen[3], Rafal E. Dunin-Borkowski[3], Richard E. Palmer[2], Kari Laasonen[4], Didier Grandjean[1]*, Ewald Janssens[1], and Peter Lievens[1]*

[1] *Quantum Solid State Physics, Department of Physics and Astronomy, KU Leuven, Celestijnenlaan 200D, box 2414, BE-3001 Leuven, Belgium.*

[2] *College of Engineering, Swansea University, Bay Campus, Fabian Way, Swansea SA1 8EN United Kingdom*

[3] *Ernst Ruska-Centre for Microscopy and Spectroscopy with Electrons and Peter Grünberg Institute Forschungszentrum Jülich GmbH, Jülich 52428, Germany*

[4] *Department of Chemistry and Materials Science, Aalto University, P.O. Box 16100, FI-00076 Aalto, Finland.*

[ǂ]*These authors contributed equally: Ting-Wei Liao and Anupam Yadav*

**Email: tiwei@dtu.dk ; didier.grandjean@kuleuven.be; peter.lievens@kuleuven.be*

Supplementary Information content:

Figures S1 to S7

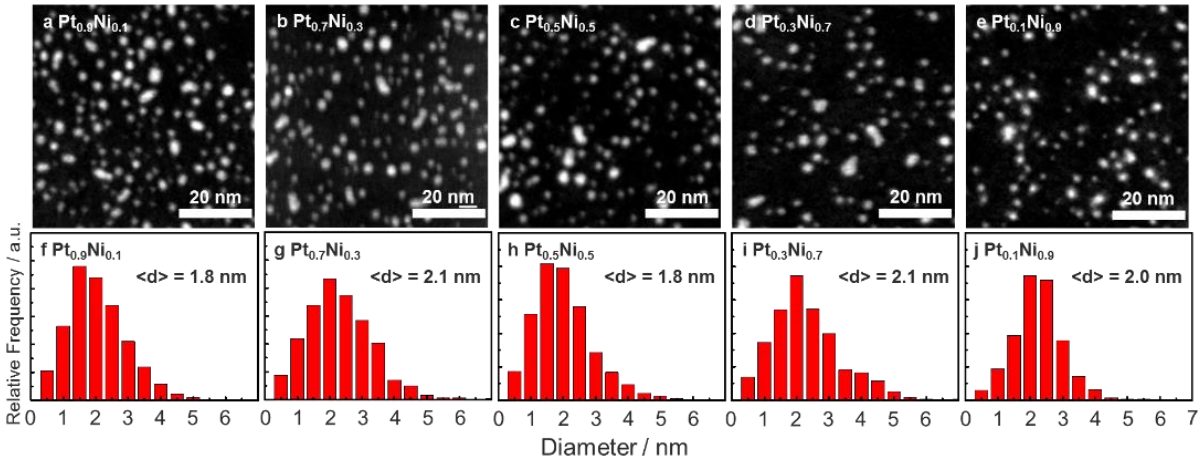

Figure S1. STEM images and histograms of diameter distributions of Pt_xNi_{x-1} BCs: (a, f) $Pt_{0.9}Ni_{0.1}$; (b, g) $Pt_{0.7}Ni_{0.3}$; (c, h) $Pt_{0.5}Ni_{0.5}$; (d, i) $Pt_{0.3}Ag_{0.7}$; (e, j) $Pt_{0.1}Ag_{0.9}$.

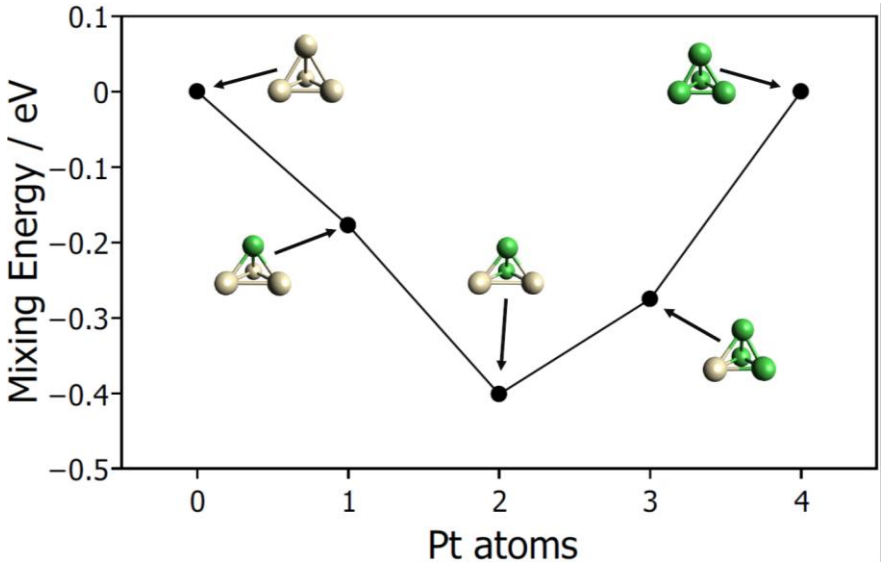

Figure S2. DFT calculations of the mixing energy of tetramers: Ni_4, Pt_1Ni_3, Pt_2Ni_2, Pt_3Ni_1, and Pt_4. The mixing energy is defined as the binding energy of mixed clusters with reference to the binding energy of their corresponding monometallic clusters. Calculations are performed at the PBE/ECP(Def2-TZVP) level.

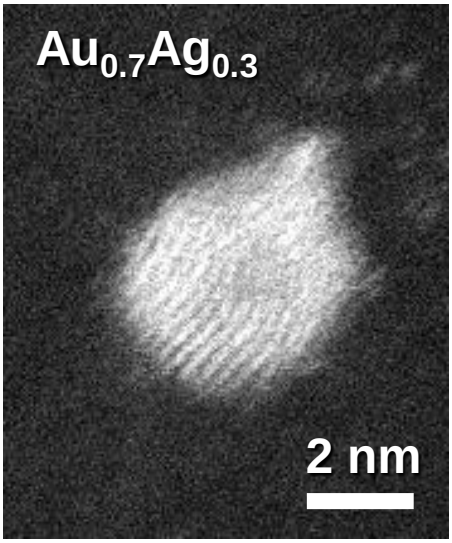

Figure S3. Atomic-scale HAADF-STEM image of $Au_{0.7}Ag_{0.3}$ BC.

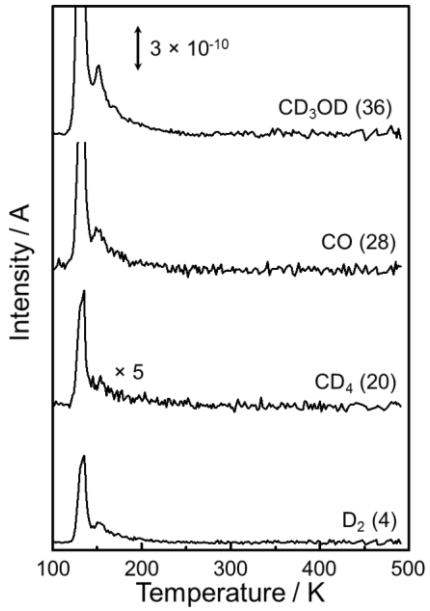

Figure S4. TPD traces for methanol-d4 desorption from the cleaned amorphous SiO_2 surface, considering the selected masses of CD_3OD (36), CO (28), CD_4 (20), D_2 (4).

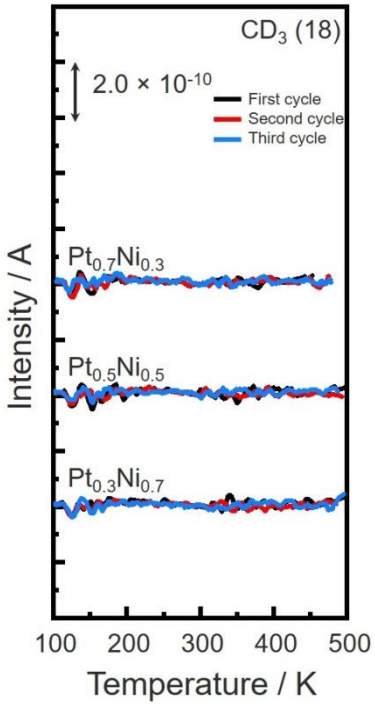

Figure S5. CD_3 mass signal (after background subtraction) measured during methanol decomposition on $Pt_{0.7}Ni_{0.3}$, $Pt_{0.5}Ni_{0.5}$ and $Pt_{0.3}Ni_{0.7}$ BCs on SiO_2 supports, showing the absence of CD_3 formation.

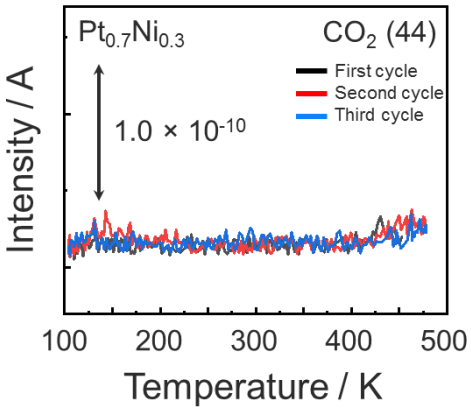

Figure S6. CO_2 signal collected during methanol decomposition on $Pt_{0.7}Ni_{0.3}$ BCs on SiO_2, showing the absence of CO_2 formation.

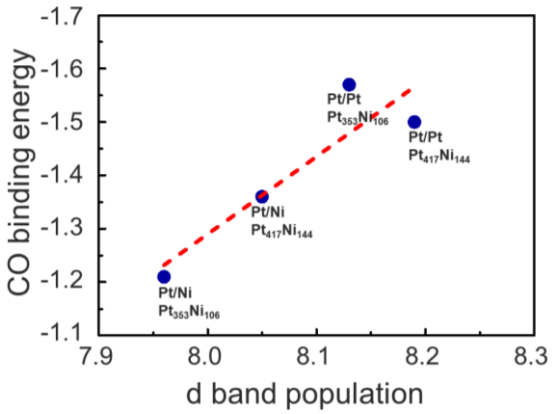

Figure S7. Overview of the CO binding energy in function of the d band population of the Pt atom on which the CO is adsorbed for Pt atoms at the (111) surface of the Wulff constructed $Pt_{353}Ni_{106}$ and larger (100) surface $Pt_{417}Ni_{144}$ BCs with either Pt or Ni subsurface atoms (blue cycles, denoted with Pt/Pt and Pt/Ni, respectively). The linear fit is present as a dash red line.

Tables S1 to S3

Table S1. CO-Pt binding energy (in eV) for various Pt adsorption sites in $Pt_{353}Ni_{106}$ and $Pt_{417}Ni_{144}$. Pt surface atoms with subsurface Ni (Pt/Ni) and subsurface Pt (Pt/Pt) are distinguished. Some of the sites with no number are unstable and some have not been calculated.

		$Pt_{353}Ni_{106}$		Pt_{459}	$Pt_{417}Ni_{144}$		Pt_{561}
		Pt/Ni	Pt/Pt	Pt	Pt/Ni	Pt/Pt	Pt
Edge	Bridge	-1.76	-1.93	-1.94	-1.82	-2.02	-2.00
100	Bridge	-1.65	-1.72	-1.69	-1.80	-1.95	-2.06
111	Bridge	-1.21	-1.57				
111	Hollow	-1.10		-1.53	-1.36	-1.50	-1.57
111	Top	-1.06	-1.46				-1.52

Table S2. d-electron population of the atoms in $Pt_{353}Ni_{106}$ and $Pt_{417}Ni_{144}$, calculated using the Löwdin and Mulliken charge analysis methods. <Ni> and <Pt> present the valence d electron population averaged over all Ni and Pt atoms in the cluster, while Pt/Ni (Pt/Pt) refer to surface Pt atoms with subsurface Ni (Pt). Pt atom on the (111) or (100) surfaces are differentiated. The values of charge Pt/X are an average value of few sites. In the $Pt_{353}Ni_{10}$ cluster, there are only two Ni atoms in a Pt/Ni (100) site. All calculations were done without adsorbed CO. The Mulliken analysis was done only for the $Pt_{353}Ni_{106}$ cluster.

	$Pt_{353}Ni_{106}$				$Pt_{417}Ni_{144}$			
	<Ni>	<Pt>	Pt/Ni	Pt/Pt	<Ni>	<Pt>	Pt/Ni	Pt/Pt
Löwdin method	8.39	8.00	7.96 (111) 8.12 (100)	8.15 (111) 8.22 (100)	8.41	7.97	8.05 (111) 7.92 (100)	8.19 (111) 8.23 (100)
Mulliken method	8.67	8.65	8.60 (111)	8.66 (111)				

Table S3. Average charges on the Pt and Ni atoms in the $Pt_{353}Ni_{106}$ and $Pt_{417}Ni_{144}$ BCs, analysed using four different charge decompositions methods: Hirchfeld method, Bader method, Löwdin method and Mulliken method. The Mulliken analysis was not performed for the larger cluster. The unit of transferred charge is the elementary charge.

	$Pt_{353}Ni_{106}$		$Pt_{417}Ni_{144}$	
	Ni	Pt	Ni	Pt
Hirchfeld method	-0.141	0.042	-0.154	0.053
Bader method	-0.284	0.085	-0.289	0.101
Löwdin method	-1.053	0.316	-1.13	0.389
Mulliken method	-0.046	0.014		

Additional material

1. Comparison of the preparation and the structure of Au-Ag BCs with Pt-Ni BCs

Series of Au_xAg_{1-x} (x=0.9 to 0.2) BCs were deposited on the same TEM, SiO_2/Si supports under identical preparation conditions (for synthesis details see method section in the main text). A similar composition-based core-shell inversion (minority element in the alloyed core and the majority element in the outer shell) was revealed using the same combination of STEM and XPS structural characterization techniques that were further verified by DFT. The STEM image $Au_{0.7}Ag_{0.3}$ (see Figure S3) shows the same core-shell architecture as that of $Pt_{0.7}Ni_{0.3}$ BCs at similar sizes. XPS peak intensities (Au 4f/Ag 3d) in Au-Ag BCs further confirmed this atomic arrangement as for Pt-Ni BCs. A similar binding energy redshift showing the reduction of the most electronegative element (Au and Pt respectively) by charge transfer from the other element is observed. The nucleation-growth processes at the origin of these structures are based on the same principle of lower mixing energy of the binary cluster present at the early stage of the BC nucleation.

2. TPD experiment and analysis procedures

First, amorphous boron doped SiO_2/Si(100) wafers, without deposited clusters, were loaded into the TPD chamber and cleaned by direct flash heating up to 700 K, in order to desorb all contaminations prior to cluster deposition. The cleaned SiO_2 samples were exposed to 5 Langmuir units (1 L = 1×10^{-6} torr seconds) of methanol-d4 at 100 K and their catalytic activity was determined by monitoring the methanol desorption as shown in Figure S4. All possible decomposed and recombined species such as CD_3OD (36), CD_3O (34), CD_2O (32), CDO (30), CO (28), CD_3 (18), CD_2 (16), CD (14), C (12), D_2 (4), CD_4 (20), D_2O (20) and CO_2 (44) were monitored in the mass spectrum. Methanol (36 u) and its cracking pattern (34 u) that desorbs at 133 K is assigned to the multilayer methanol, while the side peak at around 150 K is attributed to the monolayer methanol desorbing directly from the SiO_2 surface. The desorption of CO, CD_4/CD_3 and D_2 from the bare SiO_2 wafers that also occurs around 133 K and 150 K implies that these molecules are the products of methanol cracking and not the result of a catalytic decomposition

of methanol. As no C-O, C-D and O-D bond scission, nor C-D and C-O bond formation could be detected by the quadruple mass spectrometer (QMS) at any other temperature, bare SiO_2 was considered as an inert support towards methanol decomposition. The same inertness of all the cleaned SiO_2 supports was then verified by inspecting their methanol desorption profiles. After cleaning and examination, the supports were transferred via a home-built UHV transport vessel (base pressure in the 10^{-10} mbar range) to the CBD setup.[S1] Pt_xNi_{1-x} BCs were then deposited onto the cleaned SiO_2 supports with a precise projected surface area coverage of 25% and transferred under UHV conditions back to the TPD setup. Last, the BCs deposited samples were cooled down to 100 K and exposed to 5 L of methanol.

In our study, a quadrupole mass spectrometer has been used in the TPD experiments to detect rapidly and precisely the desorbed molecules. By using this method, we can both qualitatively and quantitatively analyse the molecules that desorb from the surface as a function of the linear temperature increase of the sample.

Since the breaking of an unreacted desorbed CD_3OD molecule generates CO and D_2 fragments contributing to the CO and D_2 signal, we applied a correction step using the CD_3OD desorption spectrum as a reference and normalizing it to that of CO/D_2 by using the methanol desorption peaks at 133 K and 150 K. In this step the real signal of CO/D_2 was obtained by subtracting CO/D_2 spectrum from the normalized CD_3OD desorption spectrum. As the detection principle of QMS is based on counting the number of ions with a corresponding m/z (mass to charge ratio), the signal intensity measured with QMS for a given molecule is proportional to the amount of the analyte molecule present in the UHV chamber. Therefore, by a simple integration of the analyte QMS signal, the amount of the desorbed molecule was determined.

Figure S5 shows the absence of CD_3 signal in $Pt_{0.7}Ni_{0.3}$, $Pt_{0.5}Ni_{0.5}$ and $Pt_{0.3}Ni_{0.7}$ BCs on SiO_2. In general C-O bond scission produces CD_3 that ultimately forms a carbon deposit that poisons the catalyst surfaces impeding the absorption of methanol. As the same activity is measured in subsequent reaction cycles the latter pathway can be safely excluded. Mechanistically, this confirms that methanol decomposition proceeds very selectively via C-D bond scission that yields only CO and D_2 (syngas) as the final products of the complete dehydrogenation of methanol.

We have further extracted from our TPD data insights on the desorption kinetics of CO from the $Pt_{0.7}Ni_{0.3}$ and pure Pt clusters surfaces. We have calculated the reaction order and CO desorption energies (E_d) using the Redheads TPD trace analysis method. [S2] We found an order of CO desorption of 1 and an E_d of CO for $Pt_{0.7}Ni_{0.3}$ BCs and pure Pt clusters of 0.85 eV and 1.18 eV, respectively when the pre-exponential factor A is 10^{14} s^{-1}, corresponding to CO interaction with Pt extended surfaces. [S3] These E_d values are in line with the CO binding energies calculated by DFT of 1.06-1.21 eV for Pt with subsurface Ni sites and 1.50-2.02 eV for Pt sites with subsurface Pt. This confirms that our Pt-Ni catalysts complete

the dehydrogenation of methanol selectively by forming exclusively CO and D_2 excluding the formation of CD_4.

3. DFT calculations

The d-electron population analysis of the BCs reveals that the electronic structure of Pt is modified by neighbouring Ni atoms. In particular, a Löwdin population analysis shows that the d-electron population of the Pt atoms is reduced by nearby Ni atoms. In $Pt_{535}Ni_{106}$, the d-electron population of the Pt atoms at the (111) surface with subsurface Pt atoms is 8.15 with subsurface Pt atoms, while that of Pt atoms with subsurface Ni atoms is only 7.96. A similar d-electron population reduction trend from subsurface Pt to subsurface Ni was observed for Pt atoms at the (100) surfaces in the $Pt_{417}Ni_{144}$ cluster (see Table S2).

References:

S1. Li, Z.; Chen, H. Y. T.; Schouteden, K.; Picot, T.; Houben, K.; Liao, T. W.; Van Haesendonck, C.; Pacchioni, G.; Lievens, P.; Janssens, E., Size-Dependent Penetration of Gold Nanoclusters through a Defect-Free, Nonporous NaCl Membrane. *Nano Lett.* **2016,** *16* (5), 3063-3070.

S2. Redhead, P. A., The effects of adsorbed oxygen on measurements with ionization gauges. *Vacuum* **1963,** *13* (7), 253-258.

S3. Zhdanov, V. P.; Pavlíček, J.; Knor, Z., Preexponential Factors for Elementary Surface Processes. *Catalysis Reviews* **1988,** *30* (4), 501-517.

S4. Singh-Miller, N.E.; Marzari, N. Surface energies, work functions, and surface relaxations of low-index metallic surfaces from first principles, *Phys. Rev. B* **2009**, *80*, 235407.